CU-CSSC-91-15

CENTER FOR SPACE STRUCTURES AND CONTROLS

EVALUATION OF DISCRETIZATION PROCEDURES FOR TRANSITION ELEMENTS IN ADAPTIVE MESH REFINEMENT

by

K. C. Park, I. Levit and G. M. Stanley

May, 1991

COLLEGE OF ENGINEERING
UNIVERSITY OF COLORADO
CAMPUS BOX 429
BOULDER, COLORADO 80309

EVALUATION OF DISCRETIZATION PROCEDURES FOR TRANSITION ELEMENTS IN ADAPTIVE MESH REFINEMENT

K. C. PARK
Center for Space Structures and Controls and
Department of Aerospace Engineering Sciences
University of Colorado
Boulder, CO 80309

and

ITZAK LEVIT AND GARY M. STANLEY
Computational Structural Mechanics Group
Lockheed Palo Alto Research Laboratory
3251 Hanover St., Palo Alto, CA 94304

May 1991

ABSTRACT

Three transition interpolation schemes for use in h or r-refinement have been analyzed in terms of accuracy, implementation ease and extendability. They include blending-function interpolation, displacement averaging, and strain matching at discrete points along the transition edge lines. The results suggest that the choice of matching depends strongly on the element formulations, (viz. displacement or assumed strain, etc.) and mesh refinement criteria employed, and to a lesser extent the choice of computer architecture (serial vs. parallel) and the equation solution procedures. A recommended paring of some of the elements with the choice factors is suggested.

1. Introduction

The h-version and/or r-version of mesh refinements have been steadily gaining popularity in recent years. A primary reason for this popularity has been due to the simplicity of data handling for subsequent refinement and solution strategies. The error estimate criteria employed for these refinements are by and large deduced from the assumption that there is no loss of accuracy in the transitional meshes or the transitional meshes are sufficiently remote from the regions of rapid stress or strain gradients (Babuska and Dorr, 1981; Felippa, 1976; Shephard and Gallagher, 1979; Zienkiewicz and Zhu, 1987). Two techniques most frequently adopted for discretizing the transitional regions are the displacement matching and the blending function interpolations (Gordon and Hall, 1973; Surana, 1980; Gordon, 1970; Cavendish and Hall, 1984).

From the viewpoint of element formulations, these techniques go well in hand with the displacement-based elements as they involve only displacements at the element boundaries. Hence, it appears that transition interpolations for other element formulations such as hybrid and assumed strain elements would require the matching of different field quantities. A recent numerical study of mesh refinement strategies that utilize displacement matching has shown that the displacement-based 9-node element yields a much better mesh refinement pattern compared to the assumed natural-coordinate strain (ANS) 9-node element (Stanley et al., 1989). This has motivated us to examine various interpolation schemes used in transition elements and classify the desirable conjugacy of element formulations vs. transition interpolation schemes.

2. Formulation of Transition Discretization

Consider two quadrilateral shell elements that have one common transition boundary as shown in Fig. 1. Although one could avoid transition nodes in triangular elements, such a strategy can lead to different nodal patterns or severe element distortion, which in turn deteriorates the accuracy in the transition regions. This is illustrated in Fig. 2. Conceivably, the distortion brought about by an h-refinement can be regularized to some extent if an r-refinement is followed up after each h-refinement. However, such an r-refinement follow-up may not contribute to overall accuracy improvements.

During the present study of transition discretizations, we will impose one important implementation requirement: the construction of transition boundary conditions should involve only the nodal degrees of freedom (dofs) along the transition element edges. If one views the nodes along the transition element edges as connectors for tying element A to elements B and C in Fig. 1, there exist three possibilities. These possibilities include blending displacement interpolation, displacement averaging, and strain (or stress) matching. We will describe in detail the three procedures.

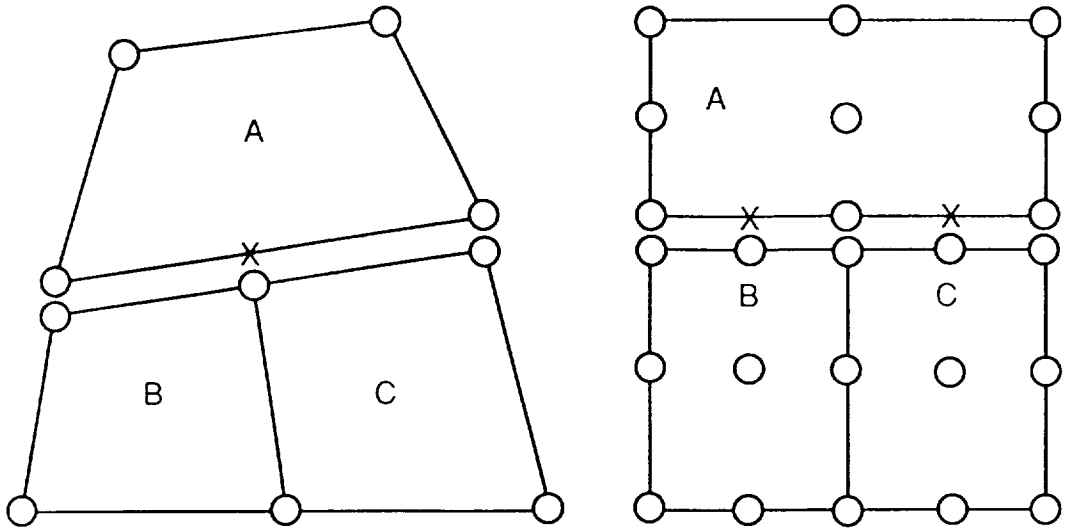

Fig. 1 **Transition Nodes for quadrilateral elements due to (h, r)-refinements**

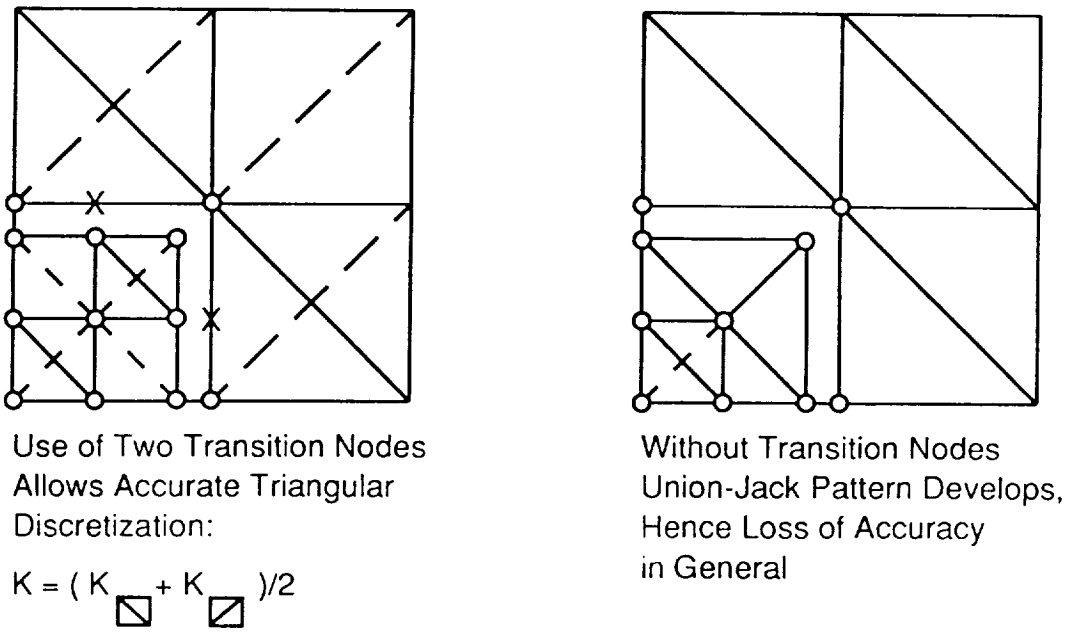

Fig. 2 **Transition Nodes vs. Union-Jack Pattern for Triangular h-Refinements**

2.1 Blending Displacement Interpolation

This is by far the simplest procedure to introduce additional nodes as connectors so that the generalized degrees of freedom associated with the additional nodes remain linearly independent of the remaining ones. For example, when a 4-node element possesses one transition edge, one introduces the following blending interpolations:

$$\mathbf{u} = \sum_{j=1}^{N} N_j(\xi, \eta) u_i \tag{1}$$

where

$$\left.\begin{aligned} N_1 &= L_1(\eta) \cdot Q_1(\xi) \\ N_2 &= L_1(\eta) \cdot Q_2(\xi) \\ N_3 &= L_2(\eta) \cdot L_1(\xi) \\ N_4 &= L_2(\eta) \cdot L_2(\xi) \\ N_5 &= L_1(\eta) \cdot Q_3(\xi) \end{aligned}\right\} \tag{2}$$

in which L's and Q's are linear and quadratic Lagrange interpolation functions. A similar blending interpolation can be constructed for a 9-node element with one or more transition edges.

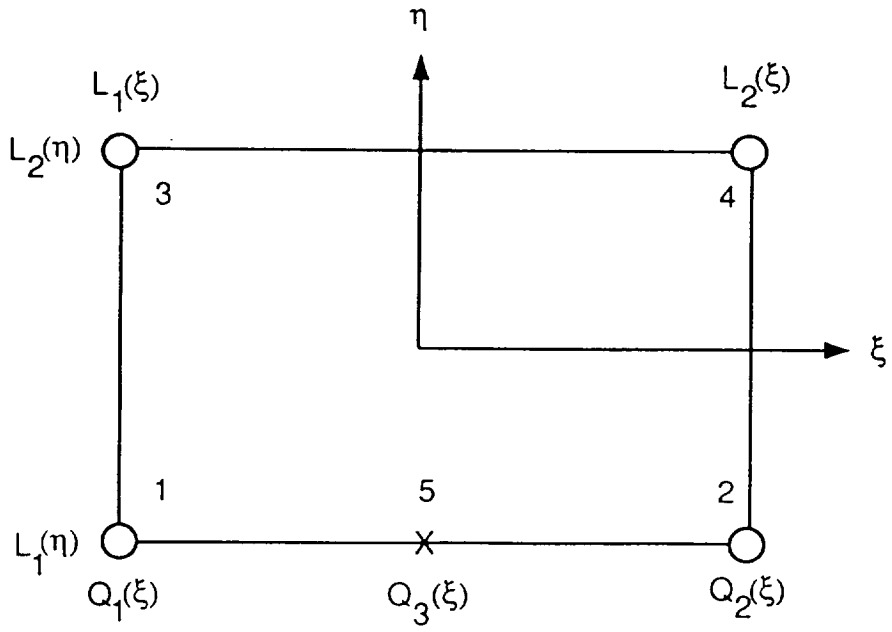

Fig. 3 Blended Interpolation of Transition Nodes

It should be pointed out that while the interpolation procedure is straightforward, the resulting element would require a (2×3)-integration rule instead of (2×2)-integration in order to preserve rank-sufficiency.

2.2 Displacement Averaging

Displacement averaging is by far the simplest procedure. For example, the displacement at node 5 can be obtained by an average of

$$\mathbf{u}_5 = \alpha \mathbf{u}_2 + (1-\alpha)\mathbf{u}_2, \qquad \alpha = \frac{\ell_1}{\ell_1 + \ell_2} \tag{3}$$

where ℓ_1 and ℓ_2 are the side length from node 1 to node 5, and node 5 to node 2, respectively. If $\ell_1 = \ell_2$, then we have

$$\Phi = \mathbf{u}_5 - \tfrac{1}{2}(\mathbf{u}_1 + \mathbf{u}_2) = 0 \tag{4}$$

Hence, $\mathbf{u}_5$ can either be eliminated or the constraint equation (4) can be augmented via the method of Lagrange multipliers ($\boldsymbol{\lambda}$) and $\mathbf{u}$ and $\boldsymbol{\lambda}$ can be solved as the system unknowns.

2.3 Strain Matching

Instead of displacement matching or interpolation, one may impose strain matching as a connector requirement. For this case, in conjunction with the present implementation requirement, viz., the use of dofs along the transition edges only, we are to match the membrane, transverse shear and bending strains:

$$\begin{aligned} \epsilon_\xi &= \frac{1}{A_\xi}\frac{\partial u_\xi}{\partial \xi} \\ \gamma_\xi &= \frac{1}{A_\xi}\frac{\partial w_\xi}{\partial \xi} + \theta_\xi \\ \kappa_\xi &= \frac{1}{A_\xi}\frac{\partial \theta}{\partial \xi} \end{aligned} \tag{5}$$

where A_ξ is the first fundamental coefficient of the neutral surface of the shell along the boundary ξ, $(u_\xi, w_\xi, \theta_\xi)$ are the tangential, normal and rotational deformation along ξ.

For a 4-node element having one transition edge as shown in Fig. 3, it turns out the strain matching is the same as the displacement averaging as long as the transition node 5 bisects nodes 1 and 2. To examine the strain matching for a 9-node case, we adopt a flat plate

for illustrative purposes as shown in Fig. 4.

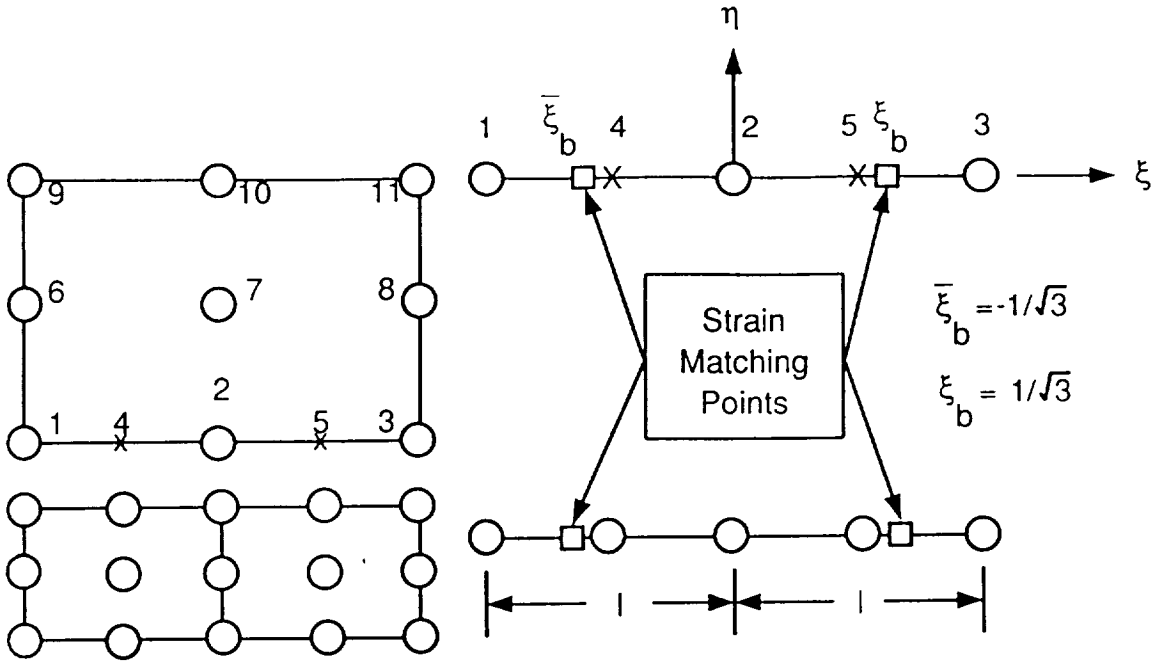

Fig. 4 Strain Matching Along A 9-Node Edge

Since there are two transition nodes with (u, w, θ_η)-dofs affected, a total of six constraints are required in order to eliminate them. Hence, we must enforce the strain matching of the three strain states given by (5) at two locations along the transition edge. Among several candidates, it has been determined that the most desirable strain-matching locations are the two Barlow points ($\xi = \pm 1/\sqrt{3}$). Matching the strains at the two Barlow points yields the following constraints:

$$\Phi = \begin{cases} 8u_4 - (3u_1 + 6u_2 - u_3) = 0 \\ 8u_5 - (-u_1 + 6u_2 + 3u_3) = 0 \\ 8v_4 - (3v_1 + 6v_2 - v_3) = 0 \\ 8v_5 - (-v_1 + 6v_2 + 3v_3) = 0 \\ 8\theta_4 - (3\theta_1 + 6\theta_2 - \theta_3) = 0 \\ 8\theta_5 - (-\theta_1 + 6\theta_2 + 3\theta_3) = 0 \\ 8\beta_4 - (3\beta_1 + 6\beta_2 - \beta_3) = 0 \\ 8\beta_5 - (-\beta_1 + 6\beta_2 + 3\beta_3) = 0 \\ 8w_4 - (3w_1 + 6w_2 - w_3) + \dfrac{\ell}{2}(\theta_3 - 2\theta_2 + \theta_1) = 0 \\ 8w_5 - (-w_1 + 6w_2 + 3w_3) - \dfrac{\ell}{2}(\theta_3 - 2\theta_2 + \theta_1) = 0 \end{cases} \tag{6}$$

Rewriting (6), one obtains

$$B_S \mathbf{d} = 0, \qquad \mathbf{d} = \lfloor u_1 \; v_1 \; w_1 \; \theta_1 \; \beta_1, \quad \ldots, \quad \ldots, \quad \ldots, \quad u_5 \; v_5 \; w_5 \; \theta_5 \; \beta_5 \rfloor^T \tag{7}$$

If the displacement averaging is adopted, one replaces the two strain constraint equations on the transverse shear strains by

$$\begin{cases} 8w_4 - (3w_1 + 6w_2 - w_3) = 0 \\ 8w_5 - (-w_1 + 6w_2 + 3w_3) = 0 \end{cases} \tag{8}$$

3. Implementation

There are two distinct needs for implementing the blending function approach vs the method of Lagrange multipliers. We shall describe the two procedures separately.

3.1 Blended Assumed Natural-Coordinate Strains

To illustrate the blended assumed natural-coordinate strain (ANS) interpolation, let us consider the following 5-noded membrane square element.

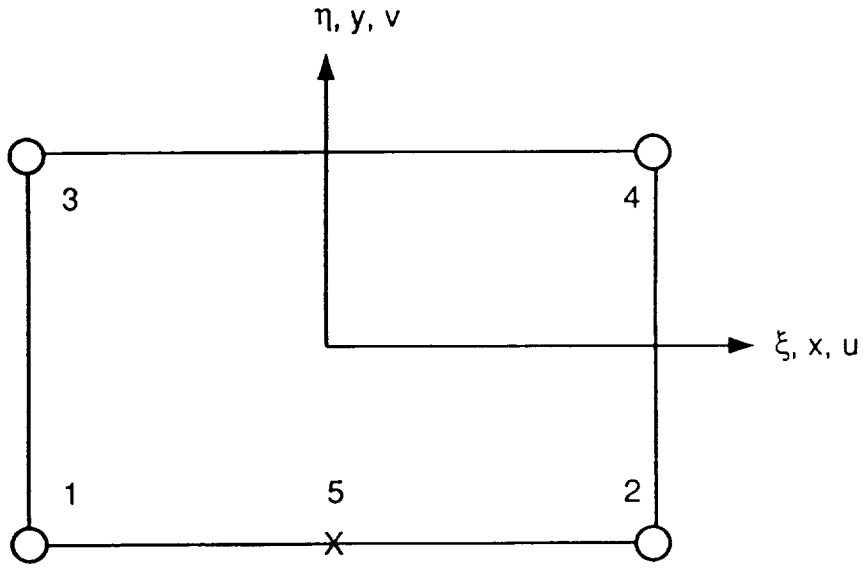

Figure 5 5-Node Blended-Function Square Plate Element

From the above figure one readily obtains the following strain expressions:

$$\left.\begin{aligned} \epsilon_{xx}|_{\eta=-1} &= \frac{u_2-u_1}{\ell}+\frac{2\xi}{\ell}(u_1+u_2-2u_5), \quad \epsilon_{xx}|_{\eta=+1}=\frac{u_4-u_3}{\ell}, \\ \epsilon_{yy}|_{\xi=-1} &= \frac{v_3-v_1}{\ell}, \quad \epsilon_{yy}|_{\xi=1}=\frac{v_4-v_2}{\ell} \\ \epsilon_{xy}|_{(\eta=0,\xi=0)} &= \tfrac{1}{2}\left(\frac{u_4-u_2}{\ell}+\frac{u_3-u_1}{\ell}\right)+\tfrac{1}{2}\left(\frac{v_4-v_3}{\ell}+\frac{v_2-v_1}{\ell}\right) \end{aligned}\right\} \tag{9}$$

To see whether (9a) yields a rank-sufficient stiffness matrix, it is adequate to check

$$K_{\epsilon_{xx}} = \int_V B_{xx}^T E B_{xx}\, dV \tag{10}$$

where

$$\epsilon_{xx} = B_{xx}\mathbf{u}, \qquad \mathbf{u} = \lfloor u_1, \quad u_2, \quad u_3, \quad u_4, \quad u_5 \rfloor^T \tag{11}$$

$$B_{xx} = \left[\, \tfrac{1}{\ell}(-1+2\xi)N_1(\eta), \quad \tfrac{1}{\ell}(1+2\xi)N_1(\eta), \quad -\tfrac{1}{\ell}N_2(\eta), \quad \tfrac{1}{\ell}N_2(\eta), \quad -\tfrac{4\xi}{\ell}N_1(\eta)\,\right] \tag{12}$$

in which

$$N_1(\eta) = \tfrac{1}{2}(1-\eta), \qquad N_2(\eta) = \tfrac{1}{2}(1+\eta)$$

and E is Young's modulus. Evaluation of (10) for a constant thickness plate (h) gives

$$K_{\epsilon_{xx}} = \frac{Eh}{18}\begin{bmatrix} 14 & 2 & 3 & -3 & -16 \\ 2 & 14 & -3 & 3 & -16 \\ 3 & -3 & 3 & -3 & 0 \\ -3 & 3 & -3 & 3 & 0 \\ -16 & -16 & 0 & 0 & 128 \end{bmatrix} \tag{13}$$

which has the required correct rank since there is only one physical rigid mode. Hence, (2 × 2)-integration of the transition element involving node 5 will have a correct rank. For higher order elements, e.g., 9-node element, similar ANS transition elements can be constructed.

3.2 Augmentation of Displacement Averaging or Strain Matching Condition

For linear cases, the transition conditions given by (6) or (7) can be augmented as follows:

$$\delta\Pi = \delta\mathbf{u}^T\mathbf{K}\mathbf{u} + \delta\boldsymbol{\lambda}^T\mathbf{B}\mathbf{u} + \delta\mathbf{u}^T\mathbf{B}^T\boldsymbol{\lambda} - \delta\mathbf{u}^T\mathbf{f} = 0 \tag{14}$$

so that one obtains

$$\begin{bmatrix} \mathbf{K} & \mathbf{B}^T \\ \mathbf{B} & 0 \end{bmatrix}\begin{Bmatrix} \mathbf{u} \\ \boldsymbol{\lambda} \end{Bmatrix} = \begin{Bmatrix} \mathbf{f} \\ 0 \end{Bmatrix} \tag{15}$$

Partitioning $\mathbf{u}$ further into the transition node $\mathbf{u}_t$ and the original node $\mathbf{u}_0$, (15) can be rearranged as

$$\begin{bmatrix} \mathbf{K}_{oo} & \mathbf{K}_{ot} & \mathbf{B}_o^T \\ \mathbf{K}_{to} & \mathbf{K}_{tt} & \mathbf{B}_t^T \\ \mathbf{B}_o & \mathbf{B}_t & 0 \end{bmatrix} \begin{Bmatrix} \mathbf{u}_o \\ \mathbf{u}_t \\ \boldsymbol{\lambda} \end{Bmatrix} = \begin{Bmatrix} \mathbf{f}_o \\ \mathbf{f}_t \\ 0 \end{Bmatrix} \tag{16}$$

So that (15) can be solved directly or by

$$\hat{\mathbf{K}}_{oo}\mathbf{u}_o = \hat{\mathbf{f}}_o \tag{17}$$

where

$$\begin{aligned} \hat{\mathbf{K}}_{oo} &= \mathbf{K}_{oo} - \mathbf{K}_{ot}\mathbf{B}_t^{-1}\mathbf{B}_o - \mathbf{B}_o^T\mathbf{B}_t^{-T}\mathbf{K}_{to} + \mathbf{B}_o^T\mathbf{B}_t^{-T}\mathbf{K}_{tt}\mathbf{B}_t^{-1}\mathbf{B}_o \\ \hat{\mathbf{f}} &= \mathbf{f}_o - \mathbf{B}_o^T\mathbf{B}_t^{-T}\mathbf{f}_t \end{aligned} \tag{18}$$

4. Strain Matching for 9-ANS Transition Element

As alluded to in Introduction, the ANS family of shell elements are constructed by interpolating the strains along the element edges and certain interior natural-coordinate lines. Hence, displacement matching or blended function approach can destroy much of the good ANS element attributes. A preferred construction of transition strategies for ANS elements is to match the strains along the transition edges at some discrete points. To this end, let us consider Fig. 6 in which the element edge A is to match with the element edges B and C as shown below.

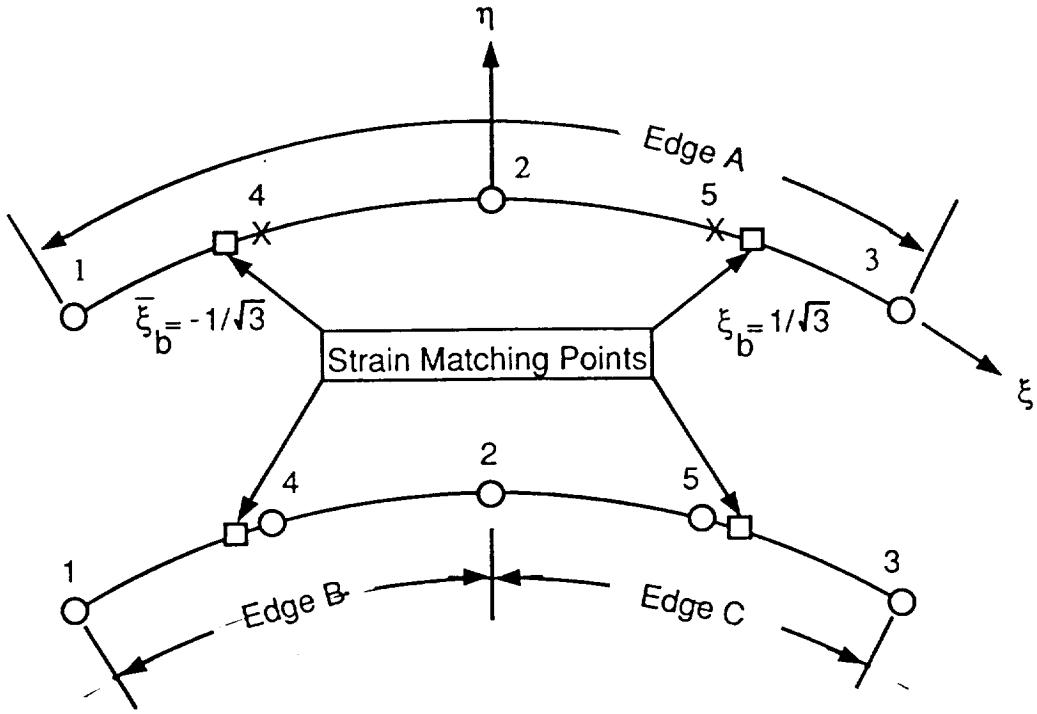

Figure 6 Strain Matching Along Three ANS Curved Element Edges

The position vector of the particle point P (Fig. 7) on the deformed shell is given by

$$\mathbf{r} = \mathbf{r}^{\circ} + \bar{\zeta}\mathbf{b}_3 \tag{19}$$

where

$$\mathbf{r}^{\circ} = x\mathbf{e}_1 + y\mathbf{e}_2 + z\mathbf{e}_3, \quad (x \;\; y \;\; z) = \{(X+u) \;\; (Y+v) \;\; (Z+w)\} \tag{20}$$

in which x, *yand* z are the ***deformed*** neutral shell surface position coordinates, (u, *vand* w) are the displacements measured in the inertial **e**-system, $\bar{\zeta}$ is the distance of the material point P from the shell neutral surface measured in the **b**-system attached on the deformed cross-section of the shell, and the vector **b** is related to the vector **e** by

$$\mathbf{b} = \mathbf{R}\mathbf{e} \tag{21}$$

The linearized (or incremental) displacement vector, $\bar{\mathbf{U}}$, is obtained from:

$$\bar{\mathbf{u}} = \mathbf{u}^T\mathbf{e} + \bar{\zeta}\hat{\mathbf{u}} \tag{22}$$

where the pseudo-rotation vector, $\hat{\mathbf{u}}$, is related to the shell-surface, pseudo-rotation quantities, $\boldsymbol{\beta}$ according to

$$\hat{\mathbf{u}} = \langle\, -\mathbf{t}_{sg}^T(2) \quad \mathbf{t}_{sg}^T(1)\,\rangle \begin{Bmatrix} \beta_1 \\ \beta_2 \end{Bmatrix}, \quad \tilde{\boldsymbol{\beta}} = \mathbf{T}_{bs}^T\tilde{\boldsymbol{\alpha}}\mathbf{T}_{bs} \tag{23}$$

in which $\mathbf{t}_{sg}^T(i)$ represents the i-th row of the transformation matrix, $\mathbf{T}_{sg}$, defined by

$$\mathbf{s} = \mathbf{T}_{sg}\mathbf{e} \tag{24}$$

that are attached to the deformed shell surface; and, $\mathbf{T}_{bs}$ relates the shell-surface basis vectors **s**, to the inertial basis vectors according to

$$\mathbf{b} = \mathbf{T}_{bs}\mathbf{s} \tag{25}$$

The covariant natural-coordinate unit vectors are then obtained by:

$$\mathbf{a}_\xi = \frac{1}{A_\xi}\frac{\partial \mathbf{r}^{\circ}}{\partial \xi} = \frac{1}{A_\xi}(x_{,\xi}\,\mathbf{e}_1 + y_{,\xi}\,\mathbf{e}_2 + z_\xi\mathbf{e}_3) = \mathbf{t}_\xi^T\mathbf{e} \tag{26}$$

$$\mathbf{a}_\eta = \frac{1}{A_\eta}\frac{\partial \mathbf{r}^{\circ}}{\partial \eta} = \frac{1}{A_\eta}(x_{,\eta}\,\mathbf{e}_1 + y_{,\eta}\,\mathbf{e}_2 + z_\eta\mathbf{e}_3) = \mathbf{t}_\eta^T\mathbf{e} \tag{27}$$

$$\mathbf{a}_\zeta = \frac{a_\xi \times a_\eta}{|a_\xi \times a_\eta|} = (x_{,\zeta}\,\mathbf{e}_1 + y_{,\zeta}\,\mathbf{e}_2 + z_{,\zeta}\,\mathbf{e}_3) = \mathbf{t}_\zeta^T\mathbf{e} \tag{28}$$

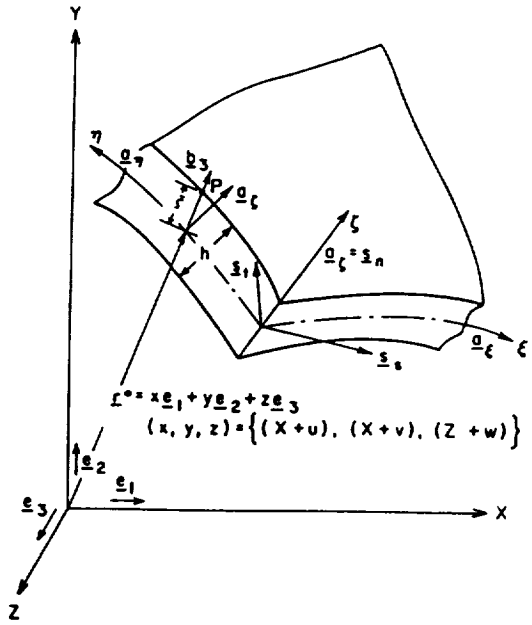

Figure 7 Geometry of Shell Surface

where the two fundamental shell surface quantities, A_ξ and A_η, are given by:

$$A_\xi^2 = \frac{\partial \mathbf{r}^\circ}{\partial \xi} \cdot \frac{\partial \mathbf{r}^\circ}{\partial \xi}, \qquad A_\eta^2 = \frac{\partial \mathbf{r}^\circ}{\partial \eta} \cdot \frac{\partial \mathbf{r}^\circ}{\partial \eta} \tag{29}$$

For subsequent applications, we express the above relation in a compact form:

$$\mathbf{a} = T_{ng}\mathbf{e} = \begin{Bmatrix} \mathbf{t}_\xi^T \\ \mathbf{t}_\eta^T \\ \mathbf{t}_\zeta^T \end{Bmatrix} \mathbf{e} \tag{30}$$

Finally, the covariant partial derivatives are given by:

$$\frac{\partial}{\partial S_\xi} = \frac{1}{A_\xi}\frac{\partial}{\partial \xi} \qquad \frac{\partial}{\partial S_\eta} = \frac{1}{A_\eta}\frac{\partial}{\partial \eta} \qquad \frac{\partial}{\partial S_\zeta} = \frac{1}{A_\zeta}\frac{\partial}{\partial \zeta} \qquad A_\zeta = h(\xi,\ \eta)/2 \tag{31}$$

where $h(\xi,\ \eta)$ is the shell thickness.

First, the membrane strains, $\epsilon_{\xi\xi}$, at the two Barlow points along the edge A are given (see Park et al.(1989) for details in the natural-coordinate strain formulation), respectively, by:

$$\epsilon_{\xi\xi}^A(\xi_b) = \frac{1}{A_{\xi_b}} \mathbf{t}_{\xi_b}^T \cdot [\tfrac{1}{2}(\mathbf{u}_3 - \mathbf{u}_1) + \xi_b(\mathbf{u}_3 - 2\mathbf{u}_2 + \mathbf{u}_1) \tag{32}$$

$$\epsilon^A_{\xi\xi}(\bar{\xi}_b) = \frac{1}{A_{\bar{\xi}_b}} \mathbf{t}^T_{\bar{\xi}_b} \cdot [\tfrac{1}{2}(\mathbf{u}_3 - \mathbf{u}_1) + \bar{\xi}_b(\mathbf{u}_3 - 2\mathbf{u}_2 + \mathbf{u}_1) \tag{33}$$

where ξ_b and $\bar{\xi}_b$ are the two right and left Barlow points along the edge A.

On the other hand, the assumed strains at the same location along the edge B and C can be derived, respectively, as

$$\epsilon^C_{\xi'\xi'}(\xi'_R) = \tfrac{1}{2}(1 + \frac{\xi'_L}{\xi'_b})\epsilon^C_{\xi'\xi'}(\xi'_b) + \tfrac{1}{2}(1 - \frac{\xi'_L}{\xi'_b})\epsilon^C_{\xi'\xi'}(\bar{\xi}'_b) \tag{34}$$

$$\epsilon^B_{\xi'\xi'}(\xi'_L) = \tfrac{1}{2}(1 + \frac{\xi'_L}{\xi'_b})\epsilon^B_{\xi'\xi'}(\xi'_b) + \tfrac{1}{2}(1 - \frac{\xi'_L}{\xi'_b})\epsilon^B_{\xi'\xi'}(\bar{\xi}'_b) \tag{35}$$

in which $\epsilon^C_{\xi'\xi'}(\xi'_b)$ and $\epsilon^C_{\xi'\xi'}(\bar{\xi}'_b)$ are the strains at the two Barlow points along the edge C, and $\epsilon^B_{\xi'\xi'}(\xi'_b)$ and $\epsilon^B_{\xi'\xi'}(\bar{\xi}'_b)$ are the strains at the two Barlow points along the edge B.

Equating $\epsilon^A_{\xi\xi}(\xi_b)$ and $\epsilon^C_{\xi'\xi'}(\xi'_L)$ one obtains the following constraint at $\xi_b = 1/\sqrt{3}$ on the edges A and C:

$$\mathbf{c}^T_5 \cdot \mathbf{u}_5 + \mathbf{c}^T_3 \cdot \mathbf{u}_3 + \mathbf{c}^T_2 \cdot \mathbf{u}_2 + \mathbf{c}^T_1 \cdot \mathbf{u}_1 = 0 \tag{36}$$

where $\mathbf{c}_i$ are given by

$$\begin{cases} \mathbf{c}_5 = (1 - \sqrt{3})\frac{1}{A^C_{\xi'_b}}\mathbf{t}^C_{\xi'_b} + (1 - 1/\sqrt{3})\frac{1}{A^C_{\bar{\xi}'_b}}\mathbf{t}^C_{\bar{\xi}'_b} \\ \mathbf{c}_3 = -(0.5 + 1/\sqrt{3})\frac{1}{A_{\xi_b}}\mathbf{t}_{\xi_b} + \frac{1}{4}(1 + \sqrt{3})\frac{1}{A^C_{\xi'_b}}\mathbf{t}^C_{\xi'_b} + \frac{1}{4}(-3 + 5/\sqrt{3})\frac{1}{A^C_{\bar{\xi}'_b}}\mathbf{t}^C_{\bar{\xi}'_b} \\ \mathbf{c}_2 = \frac{2}{\sqrt{3}}\frac{1}{A_{\xi_b}}\mathbf{t}_{\xi_b} + \frac{1}{4}(-5 + 3\sqrt{3})\frac{1}{A^C_{\xi'_b}}\mathbf{t}^C_{\xi'_b} - \frac{1}{4}(1 + 1/\sqrt{3})\frac{1}{A^C_{\bar{\xi}'_b}}\mathbf{t}^C_{\bar{\xi}'_b} \\ \mathbf{c}_1 = (0.5 - 1/\sqrt{3})\frac{1}{A_{\xi_b}}\mathbf{t}_{\xi_b} \end{cases} \tag{37}$$

where the superscript C denotes the quantities pertaining to the edge C.

Similarly, the membrane strain matching constraint at $\bar{\xi}_b = -1/\sqrt{3}$ along the edges A and B is obtained by:

$$\bar{\mathbf{c}}^T_4 \cdot \mathbf{u}_4 + \bar{\mathbf{c}}^T_3 \cdot \mathbf{u}_3 + \bar{\mathbf{c}}^T_2 \cdot \mathbf{u}_2 + \bar{\mathbf{c}}^T_1 \cdot \mathbf{u}_1 = 0 \tag{38}$$

where $\bar{\mathbf{c}}_i$ are given by

$$\begin{cases} \bar{\mathbf{c}}_4 = (1-1/\sqrt{3})\frac{1}{A^C_{\xi'_b}}\mathbf{t}^C_{\xi'_b} + (1-\sqrt{3})\frac{1}{A^C_{\bar{\xi}'_b}}\mathbf{t}^C_{\bar{\xi}'_b} \\ \bar{\mathbf{c}}_3 = (0.5-1/\sqrt{3})\frac{1}{A_{\bar{\xi}_b}}\mathbf{t}_{\bar{\xi}_b} \\ \bar{\mathbf{c}}_2 = \frac{2}{\sqrt{3}}\frac{1}{A_{\bar{\xi}_b}}\mathbf{t}_{\bar{\xi}_b} - \frac{1}{4}(1+1/\sqrt{3})\frac{1}{A^B_{\xi'_b}}\mathbf{t}^B_{\xi'_b} + \frac{1}{4}(-5+3\sqrt{3})\frac{1}{A^B_{\bar{\xi}'_b}}\mathbf{t}^B_{\bar{\xi}'_b} \\ \bar{\mathbf{c}}_1 = -(0.5+1/\sqrt{3})\frac{1}{A_{\xi_b}}\mathbf{t}_{\bar{\xi}_b} + \frac{1}{4}(-3+5/\sqrt{3})\frac{1}{A^B_{\xi'_b}}\mathbf{t}_{\xi'_b} + \frac{1}{4}(1+\sqrt{3})\frac{1}{A^B_{\bar{\xi}'_b}}\mathbf{t}^B_{\bar{\xi}'_b} \end{cases} \tag{39}$$

It should be noted that the two bending strain constraints at the two Barlow points are obtained by replacing $\mathbf{u}$ by $\hat{\mathbf{u}}$ in the preceding membrane matching conditions. The remaining two strain matching conditions, viz., the transverse shear strains,

$$\gamma_\xi = \mathbf{t}^T_\zeta \frac{1}{A_\xi}\frac{\partial \mathbf{u}}{\partial \xi} + \mathbf{t}^T_\xi \hat{\mathbf{u}} \tag{40}$$

lead to the following two constraints:

$$\mathbf{d}^T_5 \cdot \mathbf{u}_5 + \mathbf{d}^T_3 \cdot \mathbf{u}_3 + \mathbf{d}^T_2 \cdot \mathbf{u}_2 + \mathbf{d}^T_1 \cdot \mathbf{u}_1 + \mathbf{e}^T_5 \cdot \hat{\mathbf{u}}_5 + \mathbf{e}^T_3 \cdot \hat{\mathbf{u}}_3 + \mathbf{e}^T_2 \cdot \hat{\mathbf{u}}_2 + \mathbf{e}^T_1 \cdot \hat{\mathbf{u}}_1 = 0 \tag{41}$$

$$\bar{\mathbf{d}}^T_4 \cdot \mathbf{u}_4 + \bar{\mathbf{d}}^T_3 \cdot \mathbf{u}_3 + \bar{\mathbf{d}}^T_2 \cdot \mathbf{u}_2 + \bar{\mathbf{d}}^T_1 \cdot \mathbf{u}_1 + \bar{\mathbf{e}}^T_4 \cdot \hat{\mathbf{u}}_4 + \bar{\mathbf{e}}^T_3 \cdot \hat{\mathbf{u}}_3 + \bar{\mathbf{e}}^T_2 \cdot \hat{\mathbf{u}}_2 + \bar{\mathbf{e}}^T_1 \cdot \hat{\mathbf{u}}_1 = 0 \tag{42}$$

where $\mathbf{d}_i$ and $\bar{\mathbf{d}}_i$ are obtained by replacing $\mathbf{t}_\xi$ with $\mathbf{t}_\zeta$, etc., into $\mathbf{c}_i$ and $\bar{\mathbf{c}}_i$, respectively, and $\mathbf{e}_i$ and $\bar{\mathbf{e}}_i$ are given by

$$\begin{cases} \mathbf{e}_5 = (1-1/\sqrt{3})\mathbf{t}^C_{\xi'_b} + \frac{1}{3}(\sqrt{3}-1)\mathbf{t}^C_{\bar{\xi}'_b} \\ \mathbf{e}_3 = -\frac{1}{6}(1+\sqrt{3})\mathbf{t}_{\xi_b} + \frac{\sqrt{3}}{6}\mathbf{t}^C_{\xi'_b} + \frac{1}{6}(\sqrt{3}-2)\mathbf{t}^C_{\bar{\xi}'_b} \\ \mathbf{e}_2 = \frac{2}{3}\mathbf{t}_{\xi_b} + \frac{1}{6}(3-2\sqrt{3})\mathbf{t}^C_{\xi'_b} + \frac{1}{6}\mathbf{t}^C_{\bar{\xi}'_b} \\ \mathbf{e}_1 = -\frac{1}{6}(1-\sqrt{3})\mathbf{t}_{\xi_b} \end{cases} \tag{43}$$

$$\begin{cases} \bar{\mathbf{e}}_4 = \frac{1}{3}(\sqrt{3}-1)\mathbf{t}^B_{\xi'_b} + (1-1/\sqrt{3})\mathbf{t}^B_{\bar{\xi}'_b} \\ \bar{\mathbf{e}}_3 = -\frac{1}{6}(1-\sqrt{3})\mathbf{t}_{\bar{\xi}_b} \\ \bar{\mathbf{e}}_2 = \frac{2}{3}\mathbf{t}_{\bar{\xi}_b} + \frac{1}{6}\mathbf{t}^B_{\xi'_b} + \frac{1}{6}(3-2\sqrt{3})\mathbf{t}^B_{\bar{\xi}'_b} \\ \bar{\mathbf{e}}_1 = -\frac{1}{6}(1+\sqrt{3})\mathbf{t}_{\bar{\xi}_b} + \frac{1}{6}(\sqrt{3}-2)\mathbf{t}^B_{\xi'_b} + \frac{\sqrt{3}}{6}\mathbf{t}^B_{\bar{\xi}'_b} \end{cases} \tag{44}$$

Finally, the displacement $\mathbf{u}_n$ and $\hat{\mathbf{u}}_n$, namely, those perpendicular to $\mathbf{t}_\xi$ and $\mathbf{t}_\zeta$ ($\mathbf{t}_n = \mathbf{t}_\zeta \times \mathbf{t}_\xi$), can be obtained by

$$\mathbf{g}^T_5 \cdot \mathbf{u}_5 + \mathbf{g}^T_3 \cdot \mathbf{u}_3 + \mathbf{g}^T_2 \cdot \mathbf{u}_2 + \mathbf{g}^T_1 \cdot \mathbf{u}_1 = 0 \tag{45}$$

$$\bar{\mathbf{g}}_4^T \cdot \mathbf{u}_4 + \bar{\mathbf{g}}_3^T \cdot \mathbf{u}_3 + \bar{\mathbf{g}}_2^T \cdot \mathbf{u}_2 + \bar{\mathbf{g}}_1^T \cdot \mathbf{u}_1 = 0 \tag{46}$$

where

$$\begin{Bmatrix} \mathbf{g}_5 \\ \mathbf{g}_3 \\ \mathbf{g}_2 \\ \mathbf{g}_1 \end{Bmatrix} = \mathbf{t}_n(\xi_b) \begin{Bmatrix} 8 \\ 1 \\ -6 \\ +3 \end{Bmatrix}, \qquad \begin{Bmatrix} \bar{\mathbf{g}}_4 \\ \bar{\mathbf{g}}_3 \\ \bar{\mathbf{g}}_2 \\ \bar{\mathbf{g}}_1 \end{Bmatrix} = \mathbf{t}_n(\bar{\xi}_b) \begin{Bmatrix} 8 \\ 1 \\ -6 \\ -3 \end{Bmatrix} \tag{47}$$

The interpolation functions for $\hat{\mathbf{u}}_n$ at the two Barlow points are the same as for $\mathbf{u}_n$.

Combining the six strain matching constraints and the four displacement interpolation conditions together, one obtains the following equation:

$$\Phi_S = \mathbf{B}_{ANS}\{\mathbf{q}\} \tag{48}$$

where $\mathbf{q}_i = (\mathbf{u}_i,\ \hat{\mathbf{u}}_i)^T$ and $\mathbf{B}_{ANS}$ is given by

$$\mathbf{B}_{ANS} = \begin{bmatrix} \mathbf{c}_1^T & \mathbf{0} & \mathbf{c}_2^T & \mathbf{0} & \mathbf{c}_3^T & \mathbf{0} & \mathbf{0} & \mathbf{0} & \mathbf{c}_5^T & \mathbf{0} \\ \mathbf{0} & \mathbf{c}_1^T & \mathbf{0} & \mathbf{c}_2^T & \mathbf{0} & \mathbf{c}_3^T & \mathbf{0} & \mathbf{0} & \mathbf{0} & \mathbf{c}_5^T \\ \mathbf{d}_1^T & \mathbf{e}_1^T & \mathbf{d}_2^T & \mathbf{e}_2^T & \mathbf{d}_3^T & \mathbf{e}_3^T & \mathbf{0} & \mathbf{0} & \mathbf{d}_5^T & \mathbf{c}_5^T \\ \mathbf{g}_1^T & \mathbf{0} & \mathbf{g}_2^T & \mathbf{0} & \mathbf{g}_3^T & \mathbf{0} & \mathbf{0} & \mathbf{0} & \mathbf{g}_5^T & \mathbf{0} \\ \mathbf{0} & \mathbf{g}_1^T & \mathbf{0} & \mathbf{g}_2^T & \mathbf{0} & \mathbf{g}_3^T & \mathbf{0} & \mathbf{0} & \mathbf{0} & \mathbf{g}_5^T \\ \bar{\mathbf{c}}_1^T & \mathbf{0} & \bar{\mathbf{c}}_2^T & \mathbf{0} & \bar{\mathbf{c}}_3^T & \mathbf{0} & \bar{\mathbf{c}}_4^T & \mathbf{0} & \mathbf{0} & \mathbf{0} \\ \mathbf{0} & \bar{\mathbf{c}}_1^T & \mathbf{0} & \bar{\mathbf{c}}_2^T & \mathbf{0} & \bar{\mathbf{c}}_3^T & \mathbf{0} & \bar{\mathbf{c}}_4^T & \mathbf{0} & \mathbf{0} \\ \bar{\mathbf{d}}_1^T & \bar{\mathbf{e}}_1^T & \bar{\mathbf{d}}_2^T & \bar{\mathbf{e}}_2^T & \bar{\mathbf{d}}_3^T & \bar{\mathbf{e}}_3^T & \bar{\mathbf{d}}_4^T & \bar{\mathbf{e}}_5^T & \mathbf{0} & \mathbf{0} \\ \bar{\mathbf{g}}_1^T & \mathbf{0} & \bar{\mathbf{g}}_2^T & \mathbf{0} & \bar{\mathbf{g}}_3^T & \mathbf{0} & \bar{\mathbf{g}}_4^T & \mathbf{0} & \mathbf{0} & \mathbf{0} \\ \mathbf{0} & \bar{\mathbf{g}}_1^T & \mathbf{0} & \bar{\mathbf{g}}_2^T & \mathbf{0} & \bar{\mathbf{g}}_3^T & \mathbf{0} & \bar{\mathbf{g}}_4^T & \mathbf{0} & \mathbf{0} \end{bmatrix} \tag{49}$$

It can be shown that the above expression reduces to the flat, straight edge case given by (6). It should also be noted that $\hat{\mathbf{u}}$ introduced in (23) must be replaced by $(\beta_1,\ \beta_2)$ in (48) in actual implementation in order to avoid singularity.

5. Discussions

The present study has examined three possible ways for discretizing the mesh transition regions. It has been shown that for four-noded elements the displacement averaging and the strain matching yield the same transition discretization expressions. For plates with straight edges discretized by nine-noded elements, the Barlow-point displacement and strain matching becomes the same except for the transverse shear strains.

The transition interpolation schemes for curved shell boundaries for the nine-noded ANS-shell element (Park and Stanley, 1895; Stanley, 1985; Park et al., 1989) has been carried in detail for implementation in h-version mesh refinement. It is noted that the transition-boundary strain matching directly affects the resulting assumed natural-coordinate strains

employed in the formulation of ANS-shell element generation. Such explicit enforcement of strain-matching conditions along the element edges is considered a distinct advantage of the ANS-shell element.

References

1. Babuska, I. and Dorr, M., Error estimates for the combined h and p versions of the finite element method, *Numerische Mathematik*, Vol. 37, 1981, pp. 257–277

2. Cavendish, J. C. and Hall, C. A., A new class of transitional blended finite elements for the analysis of solid structures, *Int. J. Numer. Methods Engrg.*, **20**, No. 2, 1984, pp. 241–254

3. Felippa, C.A., Optimization of finite element grids by direct energy search, *Applied Mathematical Modelling*, Vol 1, 1976, pp. 93-96

4. Gordon, W. J., Blending function methods of bivariate and multivariate interpolation and approximations, *SIAM J. Numer. Anal.*, **8**, 1977, pp. 158–177

5. Gordon, W. J. and Hall, C. A., Transfinite element methods – blending function interpolation over arbitrary curved element domains, *Numer. Math.*, **21**, 1973, pp. 109–129

6. Park, K. C. and Stanley, G. M., "A Curved C^0 Shell Element Based on Assumed Natural–Coordinate Strains," Journal of Applied Mechanics, Vol. 108, 1986, pp. 278–290.

7. Park, K. C. and Stanley, G. M. and Cabiness, H., "A Family of C° Shell Elements Based on Generalized Hrennikoff's Method and Assumed Natural–Coordinate Strains," in Finite Element Methods for Nonlinear Problems, Bergan P. et al, eds., Springer-Verlag, Berlin, 1986, pp. 265-282.

8. Sander, G. and Beckers, S. P., The influence of the choice of connectors in the finite element method, *Int. J. Numer. Methods Engrg.*, **11**, No. 10, 1977, pp. 1491–1505

9. Shephard, M.S., and Gallagher, R.H., *Finite Element Grid Optimization*, PVP-38, American Society of Mechanical Engineers, New York, 1979

10. Stanley, G. M., Park, K. C. and Hughes, T. J. R., "Continuum-Based Resultant Shell Elements," Finite Element Method for Plate and Shell Structures, Volume 1: Element Technology, Hughes, T. J. R. and Hinton, E., (eds.) Pineridge Press, Swansea, U. K., 1986, pp. 1-45.

11. Surana, K. S., Transition finite elements for three-dimensional stress analysis, *Int. J. Numer. Methods Engrg.*, **15**, No. 7, 1980, pp. 991–1020

12. Zienkiewicz, O.C. and Zhu, J.Z., A simple error estimator and adaptive procedure for practical engineering analysis, *Int. J. Num. Meth. Eng.*, Vol 24, 1987, pp. 337–357.